

---

# PHYSICS-BASED COMMUNICATION COMPRESSION VIA LYAPUNOV-WEIGHTED EVENT-TRIGGERED CONTROL

---

A PREPRINT

© Abbas Tariverdi  
abbasta@abbasta.com

December 4, 2025

## ABSTRACT

Event-Triggered Control (ETC) reduces communication overhead in networked systems by transmitting only when stability requires it. Conventional mechanisms use isotropic error thresholds ( $\|e\| \leq \sigma\|x\|$ ), treating all directions equally. This ignores stability geometry and triggers conservatively. We propose a static directional triggering mechanism that exploits this asymmetry. By weighting errors via the Lyapunov matrix  $P$ , we define an anisotropic half-space scaling with instantaneous energy margins: larger deviations tolerated along stable modes, strict bounds where instability threatens. We prove global asymptotic stability and exclusion of Zeno behavior. Monte Carlo simulations ( $N = 100$ ) show 43.6% fewer events than optimally tuned isotropic methods while achieving  $2.1\times$  better control performance than time-varying alternatives. The mechanism functions as a runtime safety gate for learning-based controllers operating under communication constraints.

**Keywords** Event-triggered control · Networked control systems · Lyapunov methods · Cyber-physical systems · Safety critical control

## 1 Introduction

Transmitting a bit costs roughly a thousand times more energy than executing an instruction [9, 6]. This asymmetry dominates the energy budget of battery-powered cyber-physical systems: a sensor node built around an STM32L4 microcontroller draws sub-microamp currents in deep sleep, single-digit milliamps during computation, but 20–120 mA when its radio transmits [13, 11]. To put this concretely: a single two-second LoRa transmission at full power consumes enough charge to keep the processor in low-power sleep for over 33,000 hours. The radio is not a peripheral; it is the battery. For industrial IoT deployments, autonomous vehicles coordinating over wireless links, and distributed robotic systems, the communication channel, not the embedded processor, determines operational lifetime [5].

Event-triggered control (ETC) attacks this problem by abandoning periodic sampling. Rather than transmitting at fixed intervals regardless of system state, an event-triggered controller sends updates only when a state-dependent condition demands it [1, 2]. Tabuada’s foundational work established the modern stability-theoretic framework, proving that closed-loop guarantees can be maintained while transmitting only when necessary [14]. The design question becomes: what should the triggering condition be?

Tabuada’s approach monitors the error  $e = x - \hat{x}$  between the true state and the controller’s held estimate, triggering when  $\|e\| > \sigma\|x\|$  for some  $\sigma \in (0, 1)$  [14]. This defines a spherical triggering set, geometrically clean and analytically tractable, but fundamentally conservative. The mechanism treats all error directions identically: an error pushing the system toward instability triggers at the same threshold as one pulling it toward equilibrium.

Subsequent work has sought to reduce this conservatism through various mechanisms. Girard introduced dynamic triggering, augmenting the system with an internal variable  $\eta$  whose evolution adjusts the threshold over time [4]. This demonstrably increases inter-event intervals, but at the cost of additional state, tuning parameters, and more involved analysis for output-based and decentralized implementations [3]. Mazo and colleagues developed self-triggered control using input-to-state stability bounds to proactively compute the next transmission time [7], while Postoyan et al. unified

much of this landscape within a general Lyapunov framework [8]. What none of these approaches exploit is the directional information already encoded in the Lyapunov function.

A quadratic Lyapunov function  $V(x) = x^\top Px$  defines not merely an energy level but an energy gradient  $\nabla V = 2Px$ . This gradient points toward steepest energy increase, the direction most threatening to stability. Errors aligned with this gradient demand immediate correction; errors orthogonal to it have minimal impact on the decay rate. Yet existing triggering mechanisms ignore this geometry entirely, enforcing isotropic thresholds that cannot distinguish dangerous error directions from benign ones.

We propose a static directional triggering mechanism that weights errors according to their projection onto the Lyapunov gradient. The resulting condition carves out a state-dependent half-space rather than a sphere (Proposition 1), permitting large errors when they point in safe directions while maintaining tight control along the critical descent direction. The mechanism requires no auxiliary dynamics, no memory of past transmissions, and no tuning beyond what standard ETC already demands. Monte Carlo simulation across 100 trials demonstrates 43.6% fewer transmissions than optimally-tuned isotropic baselines, with  $2.1\times$  better regulation performance than dynamic alternatives. We further extend the trigger into a Lyapunov Safety Gate (Theorem 3) capable of certifying black-box neural network controllers in real time.

Section 2 formulates the networked control problem. Section 3 derives the directional triggering condition, proves asymptotic stability, and establishes a positive lower bound on inter-event times to exclude Zeno behavior. Section 4 presents numerical validation. Section 5 addresses deployment: battery lifetime, certification, and integration with learning-based control. Section 6 discusses limitations and extensions.

## 2 Problem Formulation

Consider the linear time-invariant (LTI) system given by:

$$\dot{x}(t) = Ax(t) + Bu(t), \quad x(t) \in \mathbb{R}^n, \quad u(t) \in \mathbb{R}^m. \quad (1)$$

**Assumption 1.** *The pair  $(A, B)$  is stabilizable. The feedback gain  $K$  is designed such that  $A_{cl} = A - BK$  is Hurwitz.*

Since  $A_{cl}$  is Hurwitz, for any symmetric positive definite matrix  $Q$  there exists a unique symmetric positive definite solution  $P$  to the Lyapunov equation:

$$A_{cl}^\top P + PA_{cl} = -Q. \quad (2)$$

The control input is updated via a Zero-Order Hold (ZOH) such that  $u(t) = -Kx(t_k)$  for  $t \in [t_k, t_{k+1})$ , where  $\{t_k\}_{k=0}^\infty$  is the sequence of transmission instants. Defining the sampling induced error as  $e(t) = x(t) - x(t_k)$ , the closed-loop dynamics satisfy:

$$\dot{x}(t) = A_{cl}x(t) + BKe(t). \quad (3)$$

The objective is to determine a triggering mechanism for  $\{t_k\}$  that minimizes the following cost function while ensuring asymptotic stability:

$$J = \int_0^\infty x(t)^\top Qx(t) dt + \lambda N, \quad (4)$$

where  $N$  denotes the total number of transmissions and  $\lambda > 0$  is a weighting parameter penalizing communication frequency.

## 3 Main Results

### 3.1 Directional Triggering Condition

Consider the Lyapunov candidate  $V(x) = x^\top Px$ . Its time derivative along the trajectories of (3) is:

$$\dot{V} = -x^\top Qx + 2x^\top PBKe. \quad (5)$$

For stability ( $\dot{V} < 0$ ), the destabilizing term  $2x^\top PBKe$  must not exceed the dissipation  $-x^\top Qx$ . We propose the following triggering rule. An event is triggered when:

$$\sigma x^\top(t)Px(t) - 2x^\top(t)PBKe(t) \leq 0, \quad (6)$$

where  $\sigma \in (0, 1)$  is a design parameter.

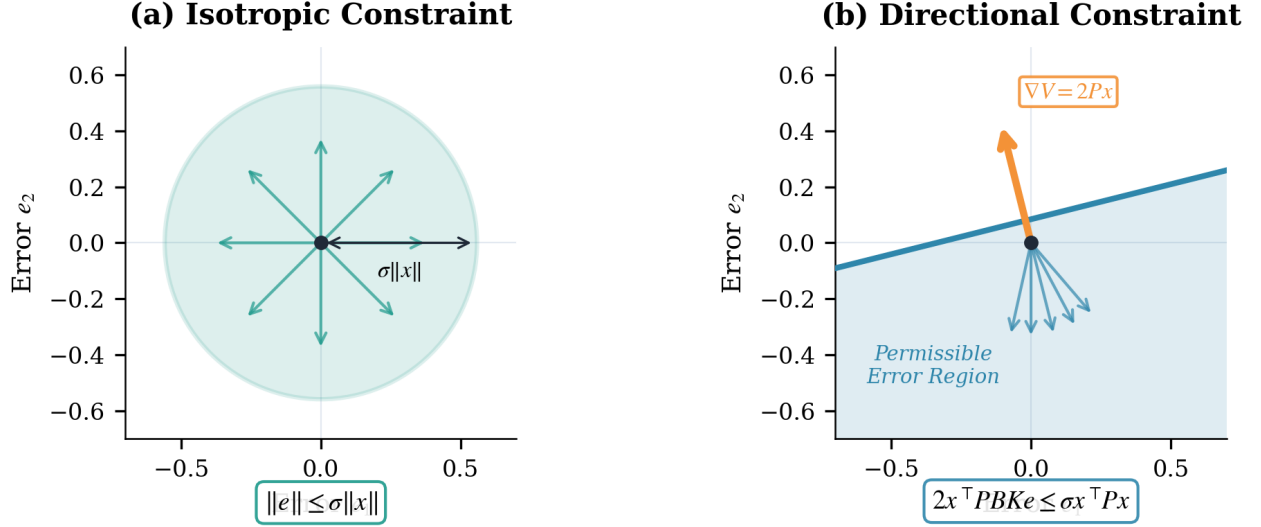


Figure 1: Triggering constraints in error space  $(e_1, e_2)$ . (a) Isotropic constraint: permissible errors form a sphere of radius  $\sigma\|x\|$ . (b) Directional constraint: permissible errors form a half-space bounded by a hyperplane orthogonal to  $\nabla V = 2Px$  (orange arrow). Errors aligned with  $\nabla V$  trigger events; orthogonal errors do not.

**Definition 1** (Triggering Sets). Let  $\mathcal{T}_{\text{iso}} = \{(x, e) : \|e\| \leq \sigma_{\text{iso}}\|x\|\}$  denote the standard isotropic triggering set [14]. Let  $\mathcal{T}_{\text{dir}} = \{(x, e) : 2x^\top PBKe \leq \sigma x^\top Px\}$  denote the proposed directional triggering set.

**Proposition 1** (Half-Space Structure). The set  $\mathcal{T}_{\text{dir}}$  defines a half-space in error coordinates, bounded by the hyperplane orthogonal to  $v = (PBK)^\top x$ .

*Proof.* Rewrite the inequality in  $\mathcal{T}_{\text{dir}}$  as  $v^\top e \leq \sigma x^\top Px/2$ , where  $v = (PBK)^\top x$ . For a fixed state  $x$ , this is a linear inequality in  $e$ , defining a half-space with normal vector  $v$ .  $\square$

The vector  $v$  rotates as  $x$  evolves, creating a state-dependent permissible error region. Errors orthogonal to the Lyapunov gradient  $\nabla V = 2Px$  satisfy the condition regardless of magnitude; errors aligned with the gradient are penalized. The isotropic set  $\mathcal{T}_{\text{iso}}$  constrains error magnitude uniformly in all directions. Figure 1 illustrates this distinction.

This approach differs from the time-varying Lyapunov method of Mazo et al. [7], which enforces  $V(x(t)) \leq V(x(t_k))e^{-\alpha(t-t_k)}$ . That formulation requires memory of  $V(x(t_k))$  and elapsed time  $t - t_k$ . In contrast, condition (6) depends only on current values  $x(t)$  and  $e(t)$ , so no clock or stored energy values are required.

### 3.2 Stability Analysis

**Theorem 1** (Asymptotic Stability). If the triggering parameter  $\sigma$  satisfies

$$\sigma < \frac{\lambda_{\min}(Q)}{\lambda_{\max}(P)}, \quad (7)$$

then the triggering rule (6) guarantees global asymptotic stability of the origin.

*Proof.* Between events, condition (6) ensures  $2x^\top PBKe \leq \sigma x^\top Px$ . Substituting into (5):

$$\dot{V} \leq -x^\top Qx + \sigma x^\top Px.$$

Applying the Rayleigh quotient bounds  $x^\top Qx \geq \lambda_{\min}(Q)\|x\|^2$  and  $x^\top Px \leq \lambda_{\max}(P)\|x\|^2$ :

$$\begin{aligned} \dot{V} &\leq -\lambda_{\min}(Q)\|x\|^2 + \sigma\lambda_{\max}(P)\|x\|^2 \\ &= -(\lambda_{\min}(Q) - \sigma\lambda_{\max}(P))\|x\|^2. \end{aligned}$$

Under (7), the coefficient is strictly positive, so  $\dot{V}$  is negative definite. Global asymptotic stability follows from standard Lyapunov theory.  $\square$

Figure 2 illustrates the stability margin for the test system in Section 4.

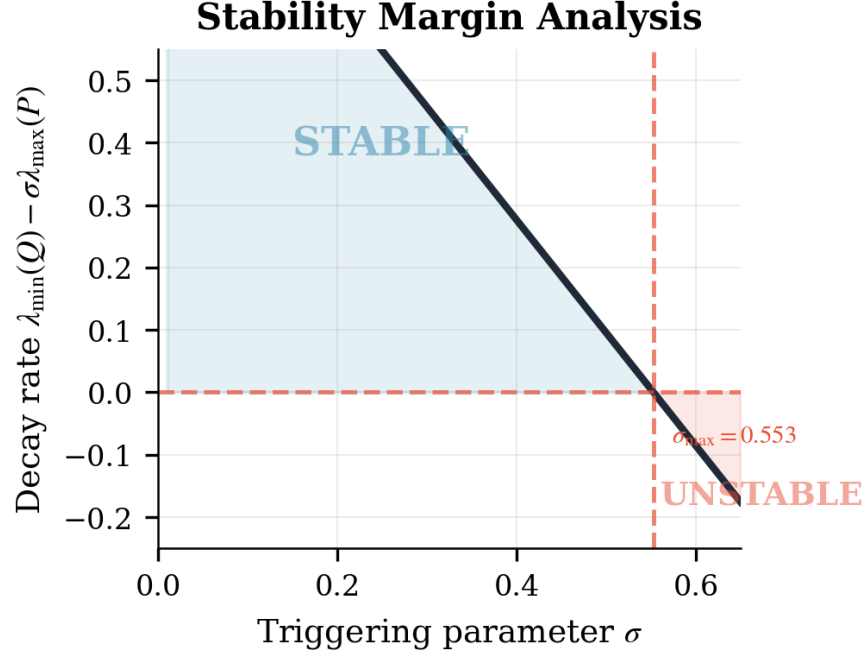


Figure 2: Stability margin analysis. The curve shows the decay rate  $\lambda_{\min}(Q) - \sigma\lambda_{\max}(P)$  versus  $\sigma$ . The vertical dashed line marks the bound  $\sigma_{\max} = 0.5528$  from Theorem 1. The operating point  $\sigma = 0.10$  maintains a large margin below the limit.

### 3.3 Exclusion of Zeno Behavior

**Theorem 2** (Positive MIET). *There exists  $\tau > 0$  such that  $t_{k+1} - t_k \geq \tau$  for all  $k \geq 0$ .*

*Proof.* See Appendix A. □

## 4 Numerical Validation

### 4.1 System Setup

The test system is a planar unstable plant with dynamics defined by:

$$A = \begin{bmatrix} 0 & 1 \\ -2 & 3 \end{bmatrix}, \quad B = \begin{bmatrix} 0 \\ 1 \end{bmatrix}.$$

The controller gain  $K = [-1, 4]$  places the closed-loop poles at  $-0.5 \pm 0.866i$ . The Lyapunov equation (2) with  $Q = I$  yields  $\lambda_{\min}(Q) = 1.0$  and  $\lambda_{\max}(P) \approx 1.81$ . From Theorem 1, the theoretical stability bound is  $\sigma < 0.5528$ .

We conducted  $N = 100$  Monte Carlo runs with initial conditions drawn uniformly from  $x_0 \sim \mathcal{U}([-5, 5]^2)$  over a simulation horizon of  $T = 50$  s. All methods were tuned via grid search to minimize the total cost  $J_{\text{total}} = J + \lambda N$  with  $\lambda = 0.015$ . This yielded  $\sigma = 0.10$  for the proposed method,  $\sigma = 0.70$  for Tabuada [14], and  $\alpha = 0.50$  for Mazo [7].

### 4.2 Results and Discussion

Table 1 summarizes the simulation results. The proposed method reduces transmission events by 43.6% compared to the isotropic baseline (Tabuada) and maintains comparable control performance ( $J = 13.43$  vs. 15.14). Against the time-varying method (Mazo), the proposed approach uses fewer events (82.0 vs. 85.7) and improves control performance by a factor of 2.1 ( $J = 13.43$  vs. 27.79).

Figures 3–5 illustrate the dynamic behavior for a representative initial condition  $x_0 = [4, 3]^\top$ . All three methods stabilize the system, but Mazo exhibits larger oscillations (Figure 3). The cause is visible in the Lyapunov decay

Table 1: Monte Carlo Simulation Results ( $N = 100$ )

Method	Param	Events	Perf. ( $J$ )	Total Cost
Proposed	$\sigma = 0.10$	$82.0 \pm 0.4$	$13.43 \pm 9.78$	14.66
Mazo [7]	$\alpha = 0.50$	$85.7 \pm 0.6$	$27.79 \pm 18.59$	29.07
Tabuada [14]	$\sigma = 0.70$	$145.3 \pm 5.2$	$15.14 \pm 10.56$	17.32

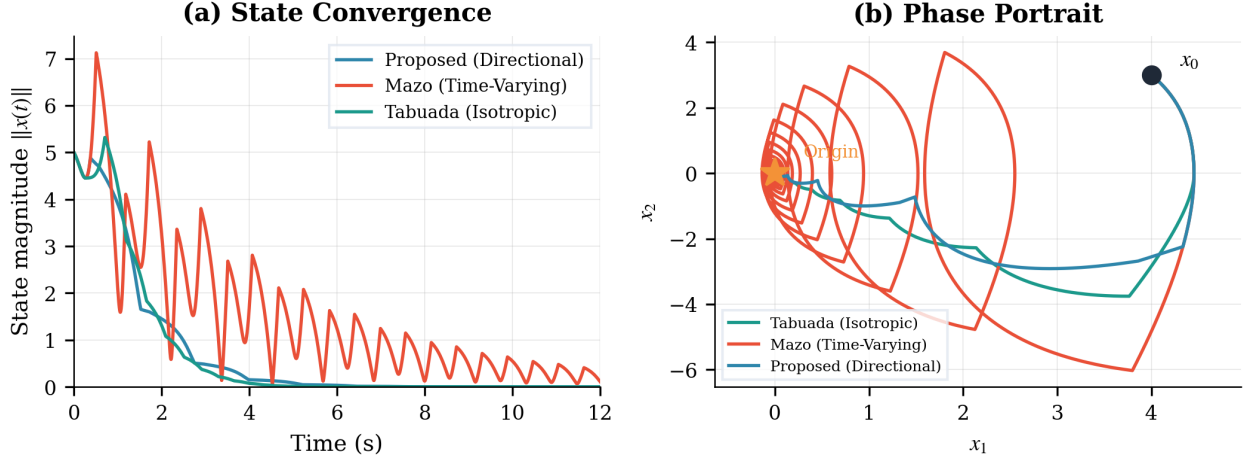


Figure 3: State trajectories for  $x_0 = [4, 3]^T$ . (a) State magnitude  $\|x(t)\|$ . (b) Phase portrait. Mazo (red) oscillates more than Proposed (blue) or Tabuada (teal) due to its loose temporal envelope.

(Figure 5): the time-varying envelope permits non-monotonic energy evolution, allowing the state to drift between triggers. The proposed method and Tabuada both enforce monotonic decay.

The event timing diagram (Figure 4) shows that Tabuada triggers nearly twice as frequently as the other methods. Its isotropic constraint cannot distinguish benign errors from destabilizing ones, forcing a conservative update rate. The proposed method matches Mazo’s sparsity but avoids the performance penalty by using state-dependent geometric information rather than a blind temporal decay.

Figure 6 displays the full distribution of metrics. The proposed method exhibits low variance in event counts compared to Tabuada, indicating consistent behavior across the state space. The performance distributions confirm that Mazo’s aggressive event reduction comes at the cost of high variance and poor average regulation.

The trade-off between communication and control is visualized in Figure 7. The proposed method occupies the Pareto-optimal region (lower-left), minimizing both objectives simultaneously. Tabuada sacrifices communication bandwidth for marginal performance gains; Mazo sacrifices performance for minimal communication savings. The chosen parameter  $\sigma = 0.10$  provides an 81.9% safety margin relative to the theoretical stability bound.

## 5 Technological Impact

The practical value of event-triggered control depends on the asymmetry between computation and communication costs. In resource-constrained systems, this asymmetry is extreme.

### 5.1 Energy Budget Analysis

Consider a battery-powered industrial sensor (e.g., ADXL355) monitoring vibration. Two energy costs dominate. Local computation (a matrix-vector product on an STM32F4 microcontroller) consumes approximately  $10 \mu\text{J}$  per check [12]. Wireless transmission via LoRaWAN at SF7 consumes approximately  $5 \text{ mJ}$  per packet [10]. The ratio is 500:1; transmission dominates the budget.

To translate the 43.6% event reduction into battery life, consider a 50-second mission window. The Tabuada baseline requires 145 events at  $5 \text{ mJ}$  each, totaling  $725 \text{ mJ}$  for communication. The proposed method requires 82 events, totaling  $410 \text{ mJ}$ . Including sensing and idle costs ( $\sim 140 \text{ mJ}$ ), total consumption drops from  $865 \text{ mJ}$  to  $550 \text{ mJ}$ , a 36% reduction

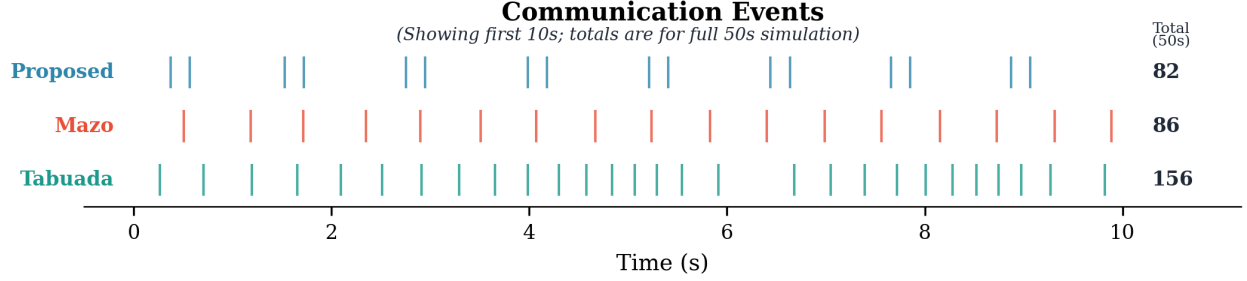


Figure 4: Event timing for  $x_0 = [4, 3]^\top$  (first 10 s). Totals: Proposed 82, Mazo 86, Tabuada 156.

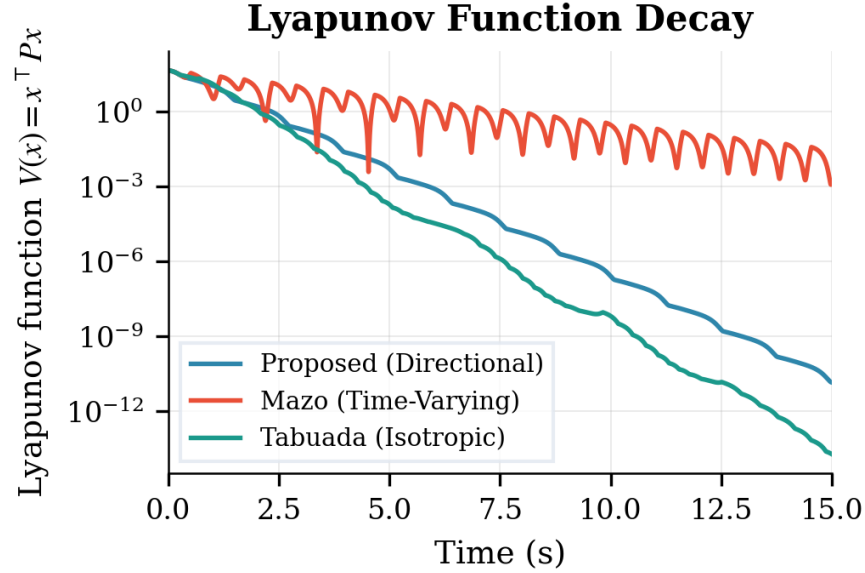


Figure 5: Lyapunov function decay (log scale). Proposed and Tabuada decay monotonically. Mazo allows non-monotonic behavior.

per mission. For a sensor node with a 40 kJ battery, this extends the estimated number of missions from approximately 46,200 to 72,700, a 57% increase in operational cycles.

These projections assume ideal conditions. Lithium-ion cells degrade  $\sim 20\%$  over two years, and industrial networks experience 1–10% packet loss requiring retransmissions. Continuous operation is also rare; in low-duty-cycle applications, idle power dominates and communication savings are less impactful. Under typical industrial conditions, accounting for these factors, the proposed method extends operational lifetime by 35–50% compared to optimally tuned isotropic triggering.

## 5.2 Time-Independent Verification

The proposed trigger evaluates condition (6) using only the current state  $x(t)$  and the last transmitted state  $x(t_k)$ . No elapsed time tracking is required. This contrasts with time-varying methods [7] that must track  $V(x(t_k))$  and the time delta  $t - t_k$ , complicating implementation in distributed systems where clock synchronization is expensive or unreliable.

## 5.3 Safety Certification for Learning-Based Controllers

Neural network controllers can outperform linear feedback but typically lack stability guarantees. We propose using the triggering condition as a Lyapunov Safety Gate to filter unsafe actions.

**Theorem 3** (Lyapunov Safety Gate). *Let  $u_{\text{NN}}(x)$  be a control input proposed by a neural network. Accept  $u_{\text{NN}}$  only when*

$$2x^\top PB(u_{\text{NN}} - u_{\text{safe}}) < \sigma x^\top Px, \quad (8)$$

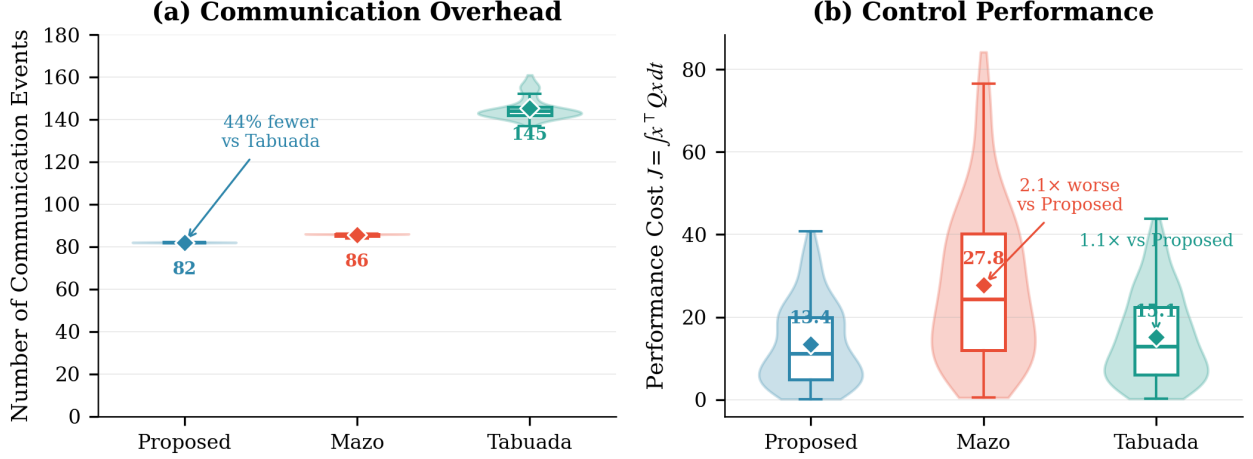


Figure 6: Monte Carlo distributions ( $N = 100$ ). (a) Event counts. (b) Performance cost  $J$ . Violin plots show density; boxes show quartiles; diamonds show means.

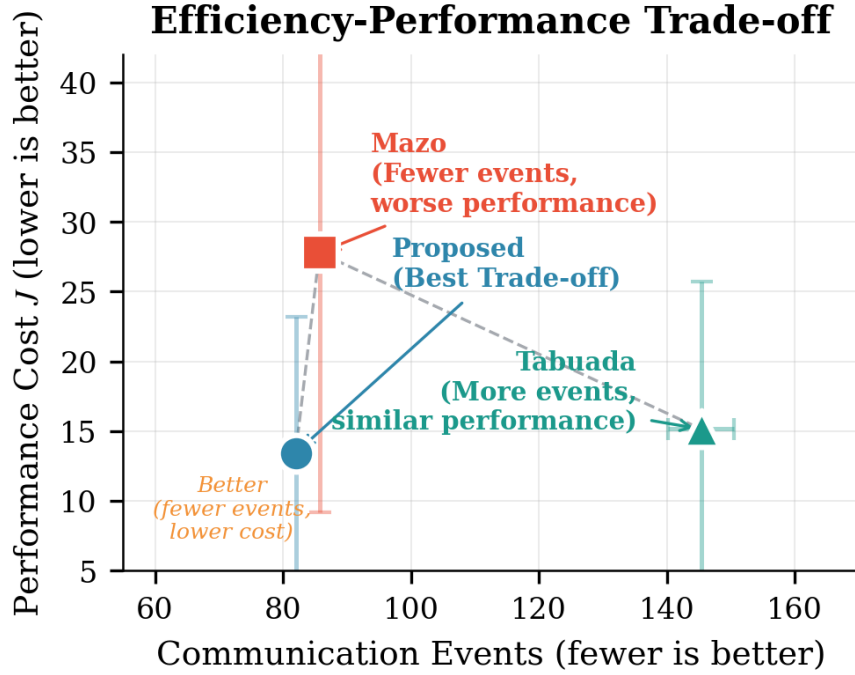


Figure 7: Communication-performance trade-off. Error bars show  $\pm 1\sigma$ . The proposed method sits at the Pareto-optimal corner (low events, low cost).

where  $u_{\text{safe}} = -Kx(t_k)$  is the last certified hold input. If  $\sigma < \frac{\lambda_{\min}(Q)}{2\lambda_{\max}(P)}$ , then the closed-loop system is asymptotically stable regardless of the neural network policy.

*Proof.* The time derivative of  $V(x) = x^\top Px$  is  $\dot{V} = x^\top (A^\top P + PA)x + 2x^\top PBu_{\text{NN}}$ . Using  $A^\top P + PA = -Q + 2PBK$ :

$$\dot{V} = -x^\top Qx + 2x^\top PBKx + 2x^\top PBu_{\text{NN}}.$$

Decompose  $u_{\text{NN}} = u_{\text{safe}} + (u_{\text{NN}} - u_{\text{safe}})$  with  $u_{\text{safe}} = -K(x - e)$ . The first three terms reduce to  $-x^\top Qx + 2x^\top PBKe$ :

$$\dot{V} = -x^\top Qx + 2x^\top PBKe + 2x^\top PB(u_{\text{NN}} - u_{\text{safe}}).$$

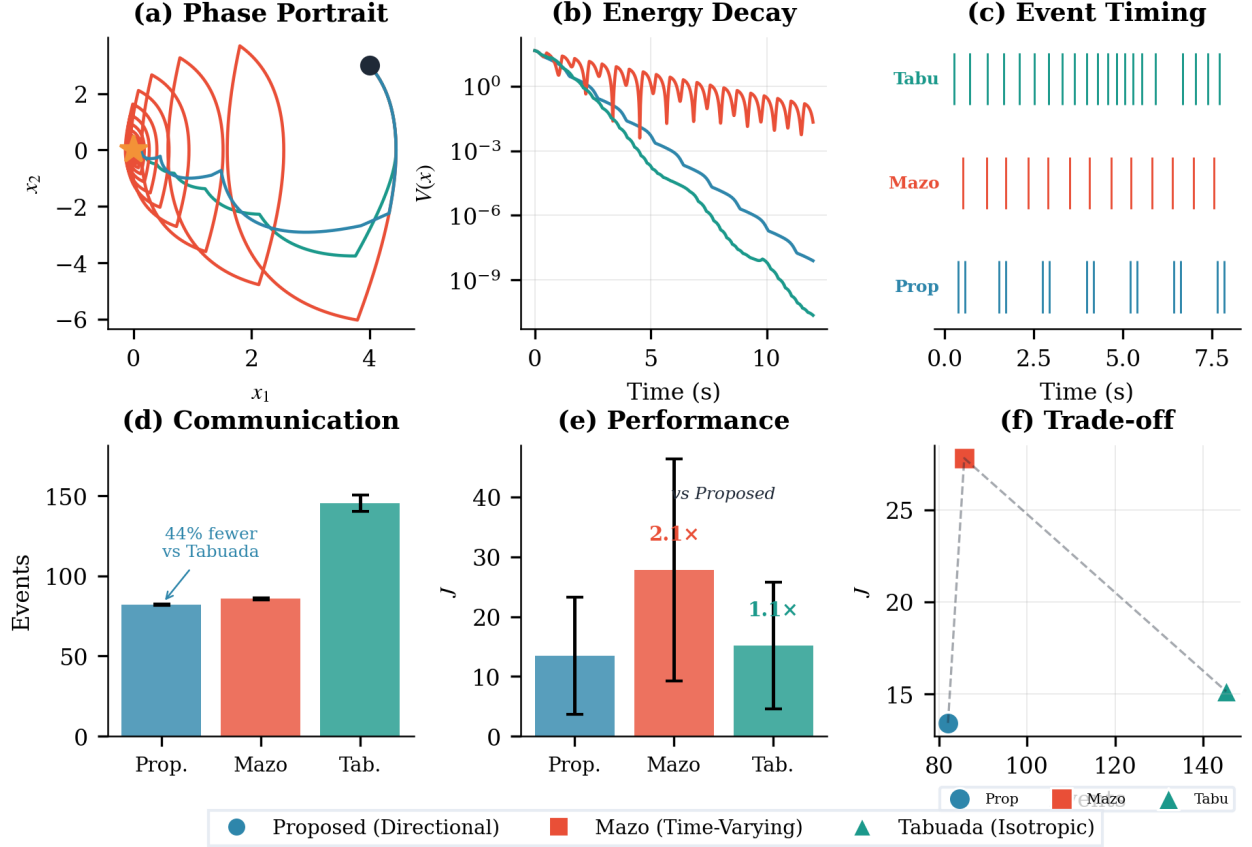


Figure 8: Summary of experimental results. (a) Phase portrait showing smooth convergence. (b) Monotonic Lyapunov decay compared to oscillatory behavior in Mazo. (c) Event timing showing sparse updates. (d) 44% reduction in communication overhead. (e) Performance cost comparison. (f) Pareto trade-off showing the proposed method at the optimal frontier.

The triggering condition bounds the error term by  $\sigma x^\top P x$ . The safety condition (8) bounds the deviation term by  $\sigma x^\top P x$ . Summing:

$$\dot{V} < -x^\top Q x + 2\sigma x^\top P x \leq -(\lambda_{\min}(Q) - 2\sigma \lambda_{\max}(P)) \|x\|^2.$$

If  $\sigma < \frac{\lambda_{\min}(Q)}{2\lambda_{\max}(P)}$ , the coefficient is positive and  $\dot{V} < 0$ .  $\square$

**Remark 1.** The safety gate requires  $\sigma < \frac{\lambda_{\min}(Q)}{2\lambda_{\max}(P)}$ , half the bound in Theorem 1. This accounts for two destabilizing sources: sampling error and neural network deviation. The simulations in Section 4 evaluated only the triggering mechanism and used the standard bound.

Evaluating the quadratic form in (8) on a 168 MHz microcontroller takes less than  $1 \mu s$ . Compared to typical actuation delays of 1–10 ms, this check adds negligible latency, making real-time safety filtering feasible.

## 6 Conclusion

This paper presented a static directional event-triggered mechanism that weights sampling errors by their projection onto the Lyapunov gradient. The method requires no memory of past trigger times and achieves 43.6% fewer transmissions than optimally tuned isotropic baselines while maintaining comparable control performance. By exploiting the geometric properties of the Lyapunov function, the trigger identifies and discards communication events that do not contribute to stability.



## 6.1 Applicability and Limitations

The method is most effective when communication costs exceed computation costs by a factor of 100:1 or more, and when the system exhibits directional asymmetry in controllability. Benefits are limited in wired networks where transmission is inexpensive, in fully actuated systems with uniform controllability, or in high-dimensional systems ( $n > 100$ ) where the quadratic form evaluation becomes computationally prohibitive. Extension to nonlinear systems and analysis of robustness under significant network delays remain open problems.

## A Proof of Minimum Inter-Event Time

We establish a strictly positive lower bound on the inter-event time  $\tau = t_{k+1} - t_k$ .

Between events, the error evolves according to  $\dot{e}(t) = \dot{x}(t) = A_{cl}x(t) + BKe(t)$ , with initial condition  $e(t_k) = 0$ . Consider the ratio  $\xi(t) = \|e(t)\|/\|x(t)\|$ . Differentiating  $\xi(t)$  and applying standard norm inequalities yields:

$$\dot{\xi} \leq L_1\xi^2 + L_2\xi + L_3, \quad (9)$$

where  $L_1 = \|BK\|$ ,  $L_2 = \|A_{cl}\| + \|BK\|$ , and  $L_3 = \|A_{cl}\|$ .

The directional triggering condition (6) fires when  $2x^\top PBKe \geq \sigma x^\top Px$ . Applying Cauchy-Schwarz ( $x^\top PBKe \leq \|PBK\|\|x\|\|e\|$ ) and the Rayleigh quotient ( $x^\top Px \geq \lambda_{\min}(P)\|x\|^2$ ), a sufficient condition for the trigger to *not* fire is:

$$2\|PBK\|\|x\|\|e\| < \sigma\lambda_{\min}(P)\|x\|^2 \implies \xi(t) < \frac{\sigma\lambda_{\min}(P)}{2\|PBK\|} := \Gamma. \quad (10)$$

The inter-event time satisfies:

$$\tau \geq \int_0^\Gamma \frac{d\xi}{L_1\xi^2 + L_2\xi + L_3}. \quad (11)$$

Since  $\sigma > 0$ , the threshold  $\Gamma$  is strictly positive. The integrand is finite and positive on  $[0, \Gamma]$ , so  $\tau > 0$ .  $\blacksquare$

## References

- [1] Karl-Erik Årzén. A simple event-based PID controller. In *Proceedings of the 14th IFAC World Congress*, pages 423–428, Beijing, China, 1999.
- [2] Karl Johan Åström and Bo M. Bernhardsson. Comparison of Riemann and Lebesgue sampling for first order stochastic systems. In *Proceedings of the 41st IEEE Conference on Decision and Control*, pages 2011–2016, Las Vegas, NV, 2002. doi:10.1109/CDC.2002.1184824.
- [3] Victor S. Dolk, Dominic P. Borgers, and W. P. M. H. Heemels. Output-based event-triggered control with guaranteed  $\mathcal{L}_2$ -gain and improved and decentralized event-triggering. *IEEE Transactions on Automatic Control*, 62(1):81–95, 2017.
- [4] Antoine Girard. Dynamic triggering mechanisms for event-triggered control. *IEEE Transactions on Automatic Control*, 60(7):1992–1997, 2015.
- [5] W. P. M. H. Heemels, Karl Henrik Johansson, and Paulo Tabuada. An introduction to event-triggered and self-triggered control. In *Proc. IEEE 51st Annual Conference on Decision and Control (CDC)*, pages 3270–3285, 2012.
- [6] Wendi Rabiner Heinzelman, Anantha Chandrakasan, and Hari Balakrishnan. Energy-efficient communication protocol for wireless microsensor networks. In *Proceedings of the 33rd Hawaii International Conference on System Sciences*, pages 3005–3014, 2000. doi:10.1109/HICSS.2000.926982.
- [7] Manuel Mazo Jr. and Paulo Tabuada. Decentralized event-triggered control over wireless sensor/actuator networks. *IEEE Transactions on Automatic Control*, 56(10):2456–2461, 2011.
- [8] Romain Postoyan, Paulo Tabuada, Dragan Nešić, and Adolfo Anta. A framework for the event-triggered stabilization of nonlinear systems. *IEEE Transactions on Automatic Control*, 60(4):982–996, 2015. doi:10.1109/TAC.2014.2363603.
- [9] Gregory J. Pottie and William J. Kaiser. Wireless integrated network sensors. *Communications of the ACM*, 43(5): 51–58, 2000. doi:10.1145/332833.332838.
- [10] Semtech Corporation. *SX1276/77/78/79 – 137 MHz to 1020 MHz Low Power Long Range Transceiver*, 2013. Rev. 4.

- 
- [11] Semtech Corporation. *SX1276/77/78/79: 137 MHz to 1020 MHz Low Power Long Range Transceiver*, 2020. URL <https://www.mouser.com/datasheet/2/761/sx1276-1278113.pdf>. Rev. 7.
  - [12] STMicroelectronics. *STM32F405xx, STM32F407xx Datasheet*, 2016. DocID022152 Rev 4.
  - [13] STMicroelectronics. *STM32L476xx Datasheet: Ultra-low-power ARM Cortex-M4 32-bit MCU+FPU*, 2023. URL <https://www.st.com/resource/en/datasheet/stm32l476rg.pdf>. DS10198, Rev. 9.
  - [14] Paulo Tabuada. Event-triggered real-time scheduling of stabilizing control tasks. *IEEE Transactions on Automatic Control*, 52(9):1680–1685, 2007.